RSC Advances

ROYAL SOCIETY OF CHEMISTRY

www.rsc.org/advances

Two- and Three-Dimensional Lanthanide-Based Coordination Polymers Assembled by the Synergistic Effect of Various Lanthanide Radii and Flexibility of a New Binicotinate-Containing Ligand: in Situ Synthesis, Structures, and Properties

Baoming Ji,[a*] Dongsheng Deng,[a] Junying Ma,[b] Chaowei Sun,[a,b] Bin Zhao[c*]

[a] *College of Chemistry and Chemical Engineering, Luoyang Normal University, Luoyang, 471022, P. R. China*

[b] *College of Chemical Engineering and Pharmaceutics, Henan University of Science and Technology, Luoyang 471003, China*

[c] *College of Chemistry and Chemical Engineering, Nankai University, Tianjin 300387, P. R. China*

ABSTRACT: Ten lanthanide coordination polymers have been obtained by the hydrothermal reactions between 3,3'-dimethoxy-2,2'-bipyridine-6,6'-dicarboxylic acid (H_2mbpdc) and rare earth ions, in which H_2mbpdc undergoes an in situ ligand transformation reaction, giving 3,3'-hydroxy-2,2'-bipyridine-6,6'-dicarboxylic acid ($hbpdcH_4$). The structures are governed by the synergistic effect of lanthanide contraction with diverse coordination modes and conformations of the ligand. They have three structural types from 3D to 2D polymers. Type **I** for large ions with the general formula $[Ln(hbpdcH)(H_2O)]_n$ (Ln = La^{III} (**1**), Ce^{III}(**2**), Pr^{III} (**3**)), possesses a 6-connected **pcu** network with unprecedented 2D entangled layers of warp-and-woof threads interwoven by left- and right-handed helical chains; type **II** for intermediate ions (Ln = Eu^{III} (**4**), Gd^{III} (**5**)) and type **III** for small ions (Ln = Tb^{III} (**6**), Dy^{III} (**7**), Ho^{III} (**8**), Er^{III} (**9**), Lu^{III} (**10**)), with general formula $[Ln(hbpdcH)(H_2O)_2]_n$. The type **II** and **III** comprised 2D Ln-hbpdcH grids. A magnetic study of **6**–**8** indicated that the coupling interaction between Ln^{3+} ions is weak. In addition, the photophysical properties of Eu and Tb polymers at room temperature were investigated.

Keywords: 3,3'-dimethoxy-2,2'-bipyridine-6,6'-dicarboxylic acid; lanthanide coordination polymers; lanthanide contraction; magnetism; photoluminescenc

* Corresponding author. Fax: +86-379-65523821. Tel: +86-379-65523821. E-mail: lyhxxjbm@126.com

Introduction

Since Weissman first discovered the photoluminescence of Eu(III) complexes in the 1940s,[1] extensive research on luminescent lanthanide complexes has been carried out.[2-4] In particular, multidimensional lanthanide-based coordination polymers (Ln–CPs) have recently gained much attention owing to their intriguing and diverse architectures[5] and potential applications in the area of catalysis, magnetism, gas storage, selective adsorption and separation, and luminescent sensors.[6] However, as high and variable coordination numbers and special characteristics lanthanide ions make it difficult to control the preparation of lanthanide complexes, the assembly of high dimensional lanthanide-based coordination polymers is currently a formidable project in contrast to the fruitful production of metal-organic frameworks (MOFs) with d-transition metal ions.[7] In general, chemists have used the coordination requirements of the metal ions, the shape and functionalities of the organic ligands, metal-to-ligand ratio, and possible counterion influence to design and synthesis of new MOFs. This strategy of crystal engineering can also be transposed successfully in lanthanide chemistry to generate novel lanthanide-based CPs. However, the assembly rule must concern the unusual coordination characteristics controlled by the radii of lanthanide ions.[8,9] As a consequences, lanthanide contraction is an effective synthetic route to fabricate diverse lanthanide complexes.[10] Recently, Liu *et al*. reported seven lanthanide-based CPs formed by 2,6-pydinedicarboxylic acid and oxalic acid, which display the progressive structural variation from high to low dimension with a decrease in the Ln^{3+} radii.[11] This interesting phenomenon was also been observed in some previous reports, and many reports are concerned with the diversity of Ln-based framework structures controlled by lanthanide contraction effect to date.[12,13]

Apart from the lanthanide contraction effect, properties of the organic ligands such as coordination mode, geometry, relative orientation of the donor groups and flexibility also play a key role in constructing Ln-based frameworks with novel structural features.[14] Generally, the utilization of low-denticity rigid organic building blocks to construct Ln–CPs often lead to the presence of solvent molecules

coordinated to the Ln^{3+} ions that results in luminescence quenching and low thermal stability. On the other hand, through the judicious choice of multidentate linkers and effective synthetic strategy, lanthanide frameworks exhibiting intense and long-lived fluorescent emissions could be achieved. So far, numerous ligands used for such a purpose have been based on polycarboxylate ligands with aromatic rings. Especially, those containing both N- and O-donors can exhibit great adaptability while coordinated to metal centers.[11-13] In this sense, pyridine-polycarboxylic acids,[15] pyrazine-polycarboxylic acids,[16] imidazole-polycarboxylic acids,[17] binicotinic acids and their derivatives[18] have been widely used as multidentate organic linkers to construct high-dimensional lanthanide CPs with fascinating architectures and potential properties. Indeed, the salient virtues inherent to the choice of binicotinic acid as multidentate ligands, including coordination polymer formation and structural reproducibility, have been highly lauded by Lombardi and others.[19] Meanwhile, rich topologies, including coordination modes, packing fashions and dimensionalities of coordination solids may be resulted from the multidentate ligand.

In this context, to fabricate novel Ln–CPs, the ligand 3,3'-dimethoxy-2,2'-bipyridine-6,6'-dicarboxylic acid (H_2mbpdc) was selected on the basis of the following reasons: (i) it is multidentate organic ligand of up to eight donor atoms-N_2O_6, which can coordinate to the metal ions in a variety of coordination modes (see Scheme 1) leading to high-dimensional structures; (ii) the two pyridine units in H_2mbpdc are linked together by a single C–C bond and they can rotate along the C–C bond to each other suggesting that the H_2mbpdc ligand has flexibility to some extent and may offer the skew coordination orientation of the carboxyl groups providing the potential for the formation of helical structures; (iii) the H_2mbpdc ligand could be transformed in situ into 3,3'-dihydroxy-2,2'-bipyridine-6,6'-dicarboxylic acid (hbpdcH_4) during the hydrothermal process, and this may be used as a deliberate strategy to produce unusual MOF architectures; (iv) compared with other binicotinic derivatives, the substituents at 3,3'-positions were found to strongly effect the geometry and the energy of the bipyridine complexes,[20] thus resulting in novel structures; (v) its hydroxyl group and carboxylate group may be partially or

completely deprotonated resulting in rich coordination modes and formation of diverse architectures. Previous studies show that H_2mbpdc is a good multidentate organic ligand for the construction of coordination polymers with Cu^{2+}.[21] However, its lanthanide complexes have never been reported to date. Following our systematic study on polycarboxylate containing lanthanide complexes, we decided to check the ability of lanthanide ions to afford high-dimensional complexes. Herein, the syntheses, structures and luminescent and magnetic properties of ten novel Ln-hbpdc CPs are reported. Single-crystal X-ray diffraction studies reveals that the ten CPs exhibit three different structure types: $[Ln(hbpdcH)(H_2O)]_n$ (Ln = La^{III} (**1**), Ce^{III}(**2**), Pr^{III} (**3**)) for type **I**, and $[Ln(hbpdch)(H_2O)_2]_n$ (Ln = Eu^{III} (**4**), Gd^{III} (**5**)) for type **II**, and $[Ln(hbpdch)(H_2O)_2]_n$ (Tb^{III} (**6**), Dy^{III} (**7**), Ho^{III} (**8**), Er^{III} (**9**), Lu^{III} (**10**) for type **III**. Remarkably, the $hbpdcH_4$ ligand in the ten Ln-CPs was in situ synthesized from H_2mbpdc through a demethylation reaction.

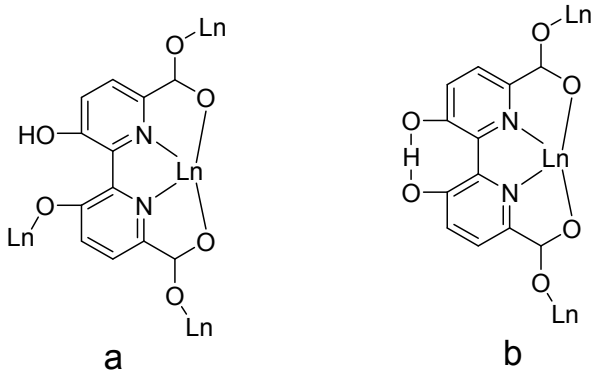

Scheme 1. The coordination modes of the $hbpdcH_4$ ligand in complexes 1-10.

Results and Discussion

Synthetic and Spectral Aspects.

Recent researches have demonstrated that the in situ ligand transformation reaction may occur during hydrothermal reaction. This may be ascribed to the features of hydrothermal synthesis, a special environment with high press and temperature, which encouraged to obtain novel CPs that are inaccessible or not easily achieved by the conventional methods.[24]. In this regard, the crystals of **1**–**10** were successfully

synthesized by reacting H_2mbpdc with the corresponding lanthanide nitrates at 180 °C for 3 days under hydrothermal conditions. It is noted that a new 3,3'-hydroxy-2,2'-bipyridine-6,6'-dicarboxylic acid ($hbpdcH_4$) ligand was generated by an in situ ligand transformation reaction of demethylation of the H_2mbpdc ligand during the hydrothermal reactions (see Scheme S1 in the Supporting Information). However, the suitable crystals were not obtained when we tried to synthesize the complexes by the use of traditional methods such as slow evaporating and diffusing at room temperature. Furthermore, some variations of the starting materials that may have influence on the assembly process including reactant molar ratio, metal salts and pH, have been investigated in details. No other kinds of crystals were obtained, however, suggesting the stability of the final structures in such temperature hydrothermal conditions.

Complexes **1**–**10** were stable towards oxygen and moisture, and were almost insoluble in common organic solvents such as $CHCl_3$, MeOH, DMSO and DMF. For example, in the polymer **6**, this result is further confirmed by the PXRD analyses (Figure S1 in the Supporting Information). The elemental analyses of **1**–**10** were consistent with their chemical formula. The IR data of **1**–**10** are reported in the Supporting Information. It can be seen that the IR spectra show features attributable to the carboxylate stretching vibrations of the complexes. The absence of signals in the range 1760–1680 cm^{-1} indicates complete deprotonation of the dicarboxylate ligand. The characteristic bands of carboxylate groups are shown in the range 1533–1578 cm^{-1} for an asymmetric stretching and 1317–1483 cm^{-1} for a symmetric stretching. The broad bands at ca. 3320 cm^{-1} are corresponding to the vibration of the water molecules in the complexes.

Structure Description.

Crystal Structure of Type I $[Ln(hbpdcH)(H_2O)]_n$ (Ln = La^{III} (1), Ce^{III}(2), Pr^{III} (3)).

X-Ray single crystal diffraction reveals that polymers **1**–**10** are isomorphous and possesses 3D network based on the linkage of unprecedented 2D entangled layers of

warp-and-woof threads interwoven by left- and right-handed helical chains, hence only the structure of complex **1** will be representatively discussed in detail. As shown in Figure 1a, the asymmetric unit of **1** consists of one unique La^{3+} ion, one $hbptcH^{3-}$ anion, one coordinated water molecule. Each La^{3+} ion is eight-coordinated, and the coordination geometry around La^{3+} ion may be described as a trigonally distorted dodecahedron. The La–O and La–N bond distances are in the range of 2.451(2)–2.638(3) Å and 2.692(2)–2.709(2) Å, respectively. The $hbpdcH^{3-}$ ligand acts as a μ_2- bridge mode to connect La^{3+} ion into two kinds of infinite 1D helical chains, right- and left-handed, as shown in Figure 1b. The 1D chains run in two nearly perpendicular directions and interweave in a 'one-over/one-under' fashion. Further, the interwoven chains are cross-linked via the chelation of the $hbpdcH^{3-}$ ligands with La ions, generating a 2D entangled woof and warp threaded layer with an uncommon topology, similar to the previous reports,[23a] as shown in Figure 1c and 1d. This kind of clothlike structure is very rare in coordination polymers and exhibits unusual structural features being that the interwoven helical chains in complex **1** have different chirality: one is left-handed while the other is right-handed, though they have the same components and linking mode. It must be pointed that the equivalent coexistence of left- and right-handed helices in **1** might due to that during the formation of helical chains, there exist an equilibrium between helices with different chirality, and no factor can provide a sufficient energy difference to move the equilibrium between left-handed and right-handed helices to one side only. Schematic representation of the 2D interwoven network is shown in Figure 1d. Furthermore, the interwoven network connects neighbouring ones with coordination bonds between hydroxyl O5 atoms and La ions to form a 3D architecture (Figure 1e). In a topological point of view, each La1–hbpdcH mononuclear motif can be regarded as six-connected nodes to connect six adjacent ones, and thus the 3D network can be simplified as a 6-connected **pcu** net,[25b] as depicted in Figure 1f.

Polymers **2** and **3** are of the same structure as **1**. The selected bond lengths and some nonbonding separations are listed in Table 1, which indicates that all the Ln–O and Ln–N bond lengths, together with the Ln···Ln separations decrease from complex

1 to complex **3**, consistent with the radius contraction from La to Pr.

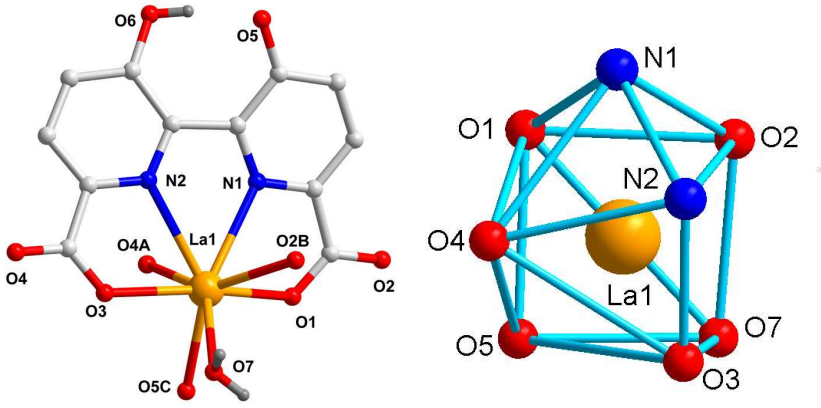

(a)

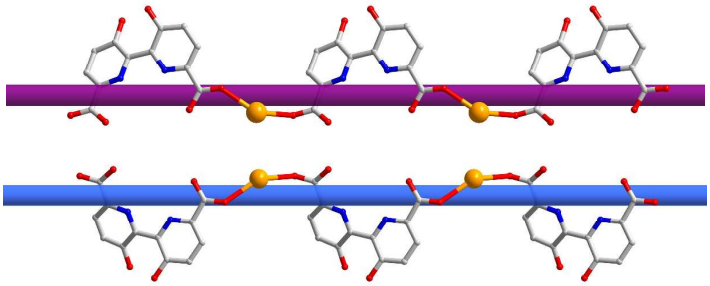

(b)

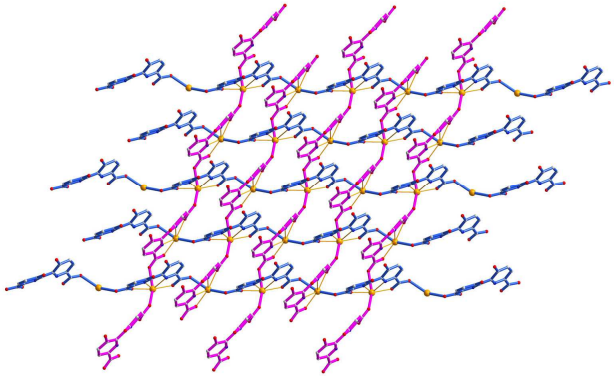

(c)

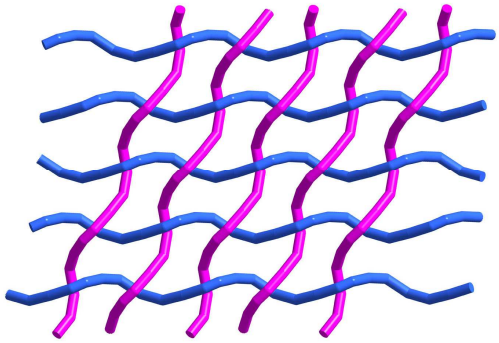

(d)

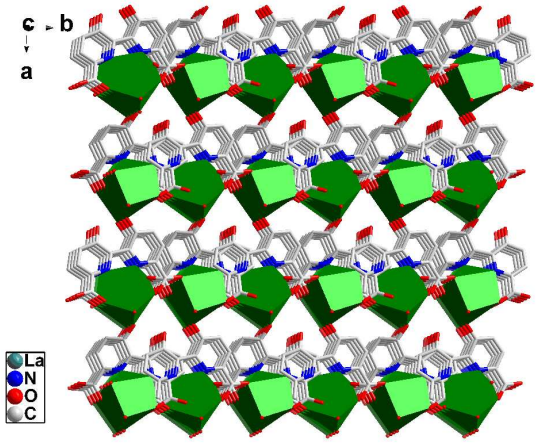

(e)

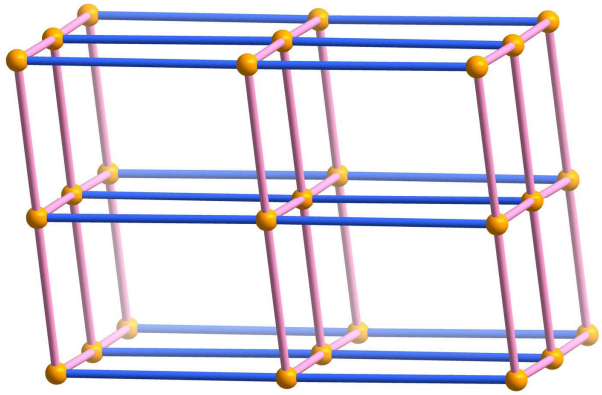

(f)

Figure 1. (a) Asymmetric unit (left) and the square-antiprismatic coordination environments of the metal ions (right) in **1** (Symmetry codes: A: x, $-y$, $z - 1/2$; B: x, $-y + 1$, $z + 1/2$; C: $x + 1/2$, $-y + 1/2$, $z + 1/2$). (b) The right- and left-handed helical chains of **1**. (c) The 2D entangled woof and warp threaded layer of **1**. (d) Schematic representation of the 2D interwoven network. (e) The 3D network of **1**. (f) Schematic representation of the **pcu** net for **1**.

Table 1. Selected Bond Lengths for Polymers **1**–**3**[a]

Bond	Distance (Å)		
	1·La	2·Ce	3·Pr
Ln–O(3A)	2.451(2)	2.416(4)	2.406(2)
Ln–O(4)	2.459(2)	2.436(3)	2.422(2)
Ln–O(1)	2.468(2)	2.441(3)	2.427(2)
Ln–O(2B)	2.477(2)	2.450(3)	2.434(2)
Ln–O(5C)	2.535(2)	2.509(3)	2.488(2)

Ln–O(7)	2.638(3)	2.628(4)	2.607(3)
Ln–N(1)	2.692(2)	2.666(3)	2.647(3)
Ln–N(2)	2.709(2)	2.680(3)	2.667(3)
doubly bridged Ln1···Ln1B	6.3144(9)	6.2998(4)	6.3005(9)
doubly bridged Ln1···Ln1C	6.4572(9)	6.4210(4)	6.3990(9)
doubly bridged Ln1···Ln1A	8.2290(2)	8.1844(7)	8.1725(2)
[a] Symmetry transformations use to generate equivalent atoms (consistent with the symmetry transformations in Figure 1a). (A): $x + 1/2, -y + 1/2, z + 1/2$; (B): $x, -y, z + 1/2$; (C): $x, -y + 1, z - 1/2$.			

Crystal Structure of Type II $[Ln(hbpdcH)(H_2O)_2]_n$ (Ln = Eu^{III} (**4**), Gd^{III} (**5**))**.**

The structure of type II, represented by complex **4** can be described as a 3D supramolecular architecture based on the linkage of 2D grid layers. As shown in Figure 2a, the asymmetric unit of **4** consists of one unique Eu^{3+} ion, one $hbptcH^{3-}$ anion, two coordinated water molecules. Each Eu^{3+} ion is eight-coordinated, in a square antiprism. One $hbpdcH^{3-}$ ligand chelates to Eu1 through two carboxylate oxygen atoms and two adjacent nitrogen atoms (O1/N1, O3/N2), occupying four coordination sites of Eu1. The remaining four coordination sites of Eu^{3+} ions are taken by the oxygen atoms of two water molecules (O7, O8) and another two $hbptcH^{3-}$ ligands, each through a single carboxylate oxygen atom (O2, O4). The Eu–O bond distances are in the range of 2.340(3)–2.427(3) Å. In the structure, the $hbpdcH^{3-}$ ligand in a tetradentate chelating mode links Eu^{3+} ion into a mononuclear Eu-hbpdcH unit, which is further connected by the carboxyl of $hbptcH^{3-}$ in a bi-monodentate μ_2-η^1:η^1-bridging mode, resulting in an alternating pattern of shorter and longer Eu···Eu distances (Figure 2b). Thus, there are two different Eu···Eu distances; the shorter one is 6.184 Å and the longer one is 6.505 Å. In addition, there are three different Eu···Eu···Eu angles; those lying among 69.93, 74.16 and 107.96°. In this way, the structure is extended parallel to the *a* axis forming a 2D coordination polymer, while considering each Eu centre as a node, a 2D 4^4 grid is formed (Figure 2b). Within the 4-membered rings, two coordinated water molecules are situated the same side of the ring, forming hydrogen bonds (see Supporting Information for detail) between their hydrogen atoms and the oxygen atoms of neighbouring

uncoordinated hydroxyl groups. As a result, a supramolecular framework is formed, as shown in Figure 2c.

Polymer **5** is isomorphous with **4**, and selected distances are listed in Table 2. As the ionic radii decreasing from Eu to Gd, all Ln–N and Ln–O bond distances decrease due to the lanthanide contraction, as do the Ln···Ln nonbonding separations spanned by the double μ_2-carboxyl bridge.

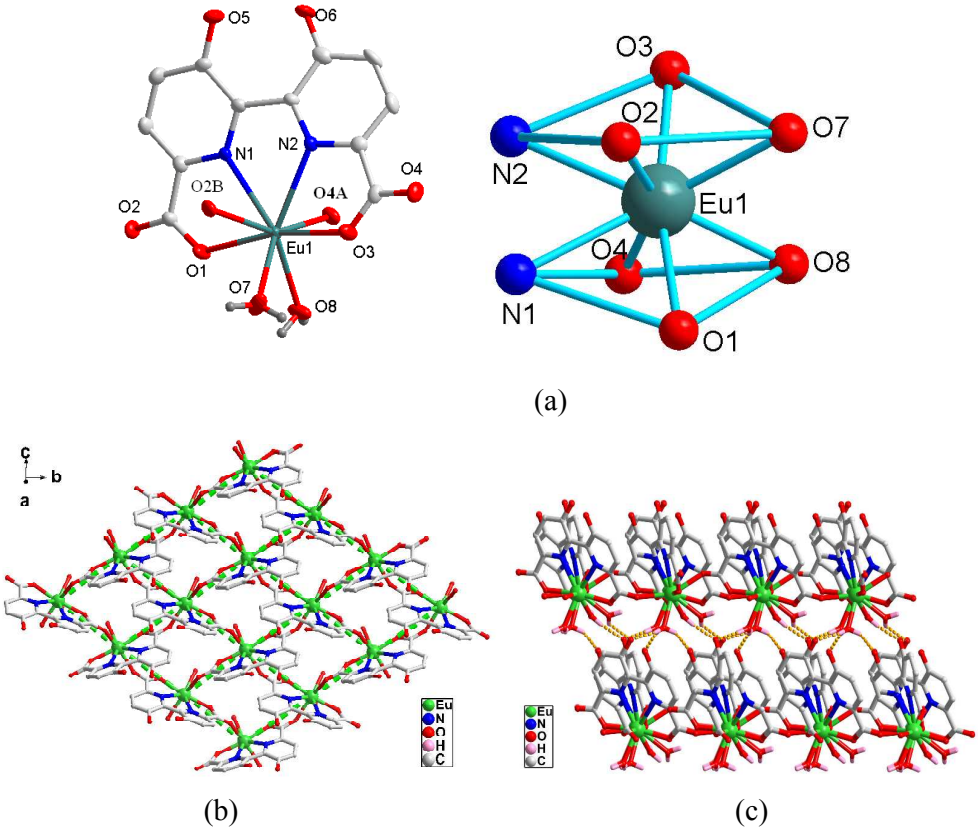

Figure 2. (a) Asymmetric unit (left) and the square-antiprismatic coordination environments of the metal ions (right) in complex **4**. (b) The 2D 4^4 grid of **4**. (c) The 3D supramolecular framework of **4**.

Table 2. **Selected Bond Lengths for Polymers 4 and 5**[a]

Bond	distance (Å)	
	4·Eu	5·Gd
Ln–O(4A)	2.340(3)	2.330(3)
Ln–O(3)	2.361(3)	2.364(3)
Ln–O(1)	2.393(3)	2.398(3)
Ln–O(8)	2.412(3)	2.402(3)
Ln–O(2B)	2.414(3)	2.407(4)

Ln–O(7)	2.427(3)	2.420(3)
Ln–N(2)	2.557(3)	2.545(3)
Ln–N(1)	2.603(3)	2.592(3)
doubly bridged Ln1···Ln1A	6.184	6.174(4)
doubly bridged Ln1···Ln1B	6.505	6.499(4)
[a] Symmetry transformations use to generate equivalent atoms (consistent with the symmetry transformations in Figure 2a). (A): x, $-y + 1$, $z - 1/2$; (B): x, $-y + 2$, $z + 1/2$.		

Crystal Structure of Type III $[Ln(hbpdcH)_{0.5}(H_2O)]_n$ (Tb^{III} (6), Dy^{III} (7), Ho^{III} (8), Er^{III} (9), Lu^{III} (10)).

The crystal structures of complexes **6**–**10** are isomorphous, belonging to the orthorhombic system with space group *Pbcn*, only complex **10** was discussed in detail as a representative. As depicted in Figure 3a, the asymmetric unit of complex **10** contains half unique Lu^{3+} ion, half $hbpdcH^{3-}$ anion, one coordinated water molecule. Each Lu^{3+} ion is eight-coordinated by two nitrogen atoms and two carboxylate oxygen atoms from one $hbptcH^{3-}$ ligand, two carboxylate oxygen atoms from the other two $hbpdcH^{3-}$ ligand and two coordinated water molecules. Its coordination geometry can be viewed as being a trigonally distorted dodecahedron. The Lu–O bond distances are in the range of 2.2327(19)–2.3931(18) Å. The average lengths of the Ln–O bonds in complexes **8** and **9** are 2.452(2) and 2.437(4) Å, respectively, in accordance with the decrease of the lanthanide metal radius.[11-13]

As shown in Figure 3b, the $hbpdcH^{3-}$ acts as a tetradentate chelating ligand to link links Lu^{3+} ion into a mononuclear Lu-hbptcH unit. Subsequently, the Lu-hbpdcH units are further interconnected by the carboxyl of the $hbptcH^{3-}$ ligands in a bi-monodentate μ_2-η^1:η^1-bridging mode to generate the 2D 4^4 grid, similar to those observed in polymers **4** and **5**. It is noted that all the Lu···Lu distances between the adjacent Lu-hbpdcH units are 6.0081(5) Å. Moreover, such 2D layers are connected by the extensive hydrogen bonds (see Supporting Information for detail) to generate a 3D supramolecular architecture, as shown in Figure 3c.

Polymers **6**, **7**, **8**, and **9** are isomorphous with 10**.** The subseries of complexes of type III structure also show the effect of lanthanide contraction: Ln–O bond lengths

and Ln···Ln nonbonding distances decrease along with the decrease of ionic radii from Tb to Lu (Table 3).

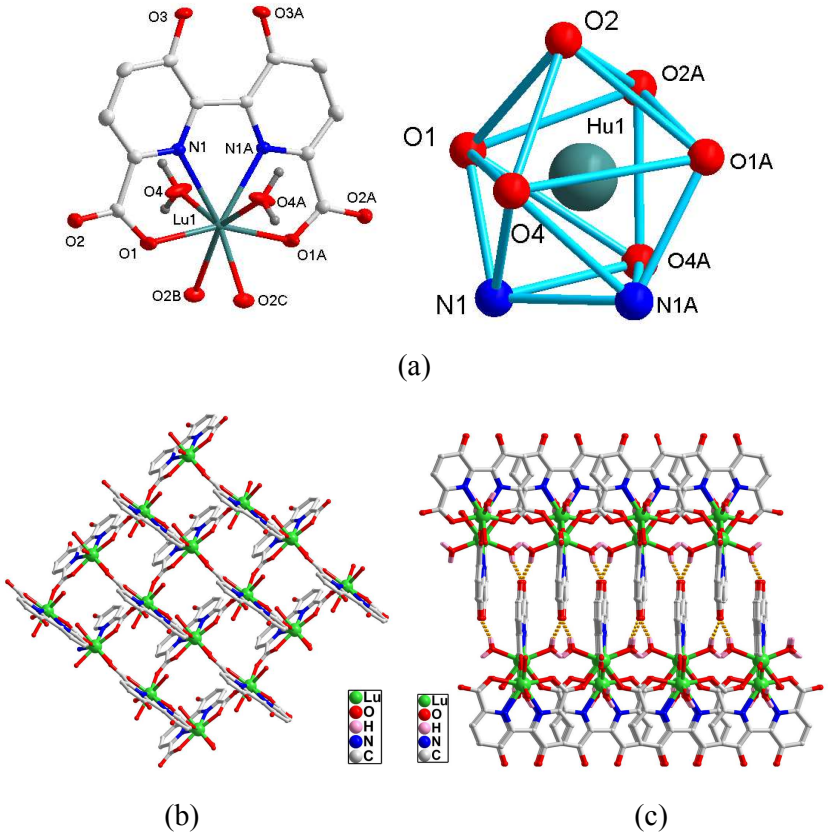

Figure 3. Asymmetric unit (left) and the square-antiprismatic coordination environments of the metal ions (right) in complex **10.** (b) The 2D 4^4 grid of **10**. (c) The 3D supramolecular framework of **10**.

Table 3. Selected Bond Lengths for Polymers 6–10[a]

bond	distance (Å)				
	6·Tb	7·Dy	8·Ho	9·Er	10·Lu
Ln–O(1)	2.286(2)	2.272(3)	2.271(2)	2.255(2)	2.2327(19)
Ln–O(1A)	2.286(2)	2.272(3)	2.271(2)	2.255(2)	2.2327(19)
Ln–O(4)	2.359(2)	2.345(3)	2.343(2)	2.323(2)	2.294(2)
Ln–O(4A)	2.359(2)	2.345(3)	2.343(2)	2.323(2)	2.294(2)
Ln–O(2B)	2.447(2)	2.432(3)	2.430(2)	2.417(2)	2.3931(18)
Ln–O(2C)	2.447(2)	2.432(3)	2.430(2)	2.417(2)	2.3931(18)
Ln–N(1A)	2.508(2)	2.494(3)	2.486(2)	2.469(2)	2.443(2)
Ln–N(1)	2.508(2)	2.494(3)	2.486(2)	2.469(2)	2.443(2)
doubly bridged Ln1···Ln1A	6.0694(4)	6.0483(4)	6.0561(3)	6.0343(3)	6.0081(5)

[a]Symmetry transformations use to generate equivalent atoms (consistent with the symmetry transformations in Figure 3a). (A): $-x$, y, $-z + 3/2$; (B): $-x + 1/2$, $-y + 1/2$, $z + 1/2$; (C): $x- 1/2$, $-y + 1/2$, $-z + 1$; (1#): –x, –y, –z+1; (2#): $x- 1/2$, $-y + 1/2$, $-z + 1$.

Comparison of the Crystal Structures.

Although polymers **6–10** were synthesized from the same starting materials and experimental method, it is interesting to observe that they present a clear progressive change in three different types of crystal structures. Type **I** structure results from the large La, Ce and Pr ions with 3D networks constructed from the left-handed and right-handed helices bridged by the organic ligands, respectively; the intermediate ions, Eu and Gd, form a type **II** structure with the distinct 2D 4^4 grid, and the small ones, Tb, Dy, Ho, Er, and Lu, afford a type **III** structure which possesses the same 2D 4^4 grid as that observed in type **II**. Thus, with the increasing atomic number of lanthanides, the structures of ten coordination polymers changed from 3D to 2D, and they display three different side views of the 3D (1–**3**), 2D (4 and 5), and 2D (**6–10),** as depicted in Figure S2 (in the Supporting Information). Most importantly, the result of comparation of the average Ln–O and Ln–N bond distances among the ten polymers (Table 1, 2, and 3) shows that the average bond lengths between the lanthanide and oxygen atoms are decreasing continuously from 2.638(3) to 2.233(19) Å, and the average bond distances between the lanthanide and nitrogen atoms are also decreasing continuously from 2.709(2) to 2.443(2) Å. In view of the above-mentions, it is the lanthanide contraction effect that results in forming the different structure, similar to the previous reports.[11-13]

Thermal Behaviors and Photoluminescent Properties.

The thermal stability of the ten polymers was investigated through TGA experiments in the temperature range of 25–900 °C under a flow of nitrogen. Since the progressive types of structures of these polymers, only three polymers in each type are selected, La of type **I**, Eu for type **II**, and Lu of type **III** for description. As depicted in Figure 4, the three types **I**, **II**, and **III** show similar thermal behaviors.

The TGA curves of type **I**, type **II** and type **III** display initial weight losses up to

137, 121 and 155 °C, respectively. The observed weight losses of 4.54% for type I, 8.05% for type II, and 7% for type III are in agreement with calculated value for the loss of coordinated water molecules (4.19% for type I, 8.35% for type II, and 7.43 for type III). The anhydrous phases are stable between 200 and 560 °C, and then the framework collapses. For example, in the polymer **10**, this result is further confirmed by the PXRD analyses (Figure S3 in the Supporting Information). It can be seen that, under 450 °C, the PXRD patterns of the different temperature are almost the same to that simulated from the single-crystal data, indicating the integrity of the framework of polymer **10** is robust to the exclusion of water.

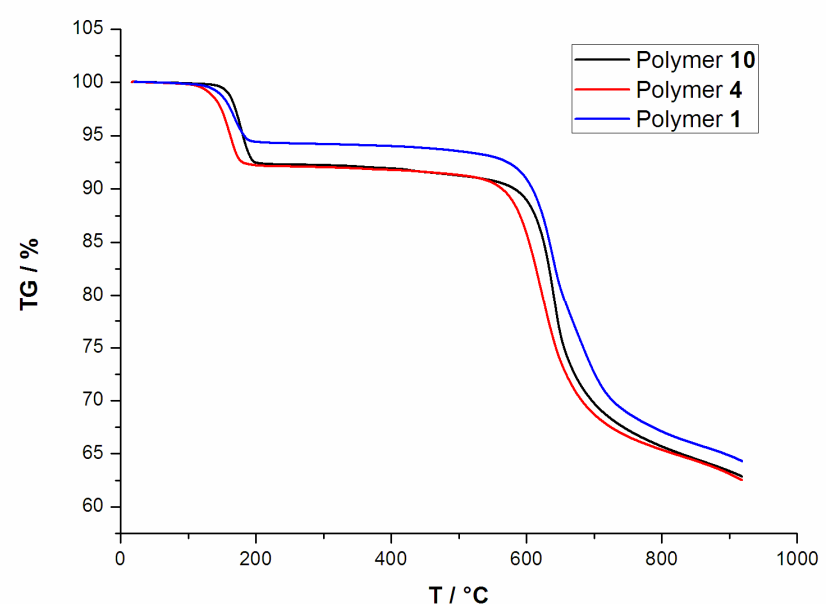

Figure 4. Thermogravimetric analyses (TGA) curves of polymers **1**, **4** and **10** under N_2 atmosphere.

The luminescent spectra of **4**, **6** and ligand in the solid were recorded at room temperature, as shown in Figure 5. For the polymer **4**, irradiated at 385 nm, the characteristic emissions of Eu(III) are obtained distinctly at the peaks of 580, 595, 621 and 701 nm, corresponding to $^5D_0 \rightarrow {}^7F_0$, $^5D_0 \rightarrow {}^7F_1$, $^5D_0 \rightarrow {}^7F_2$, and $^5D_0 \rightarrow {}^7F_4$ transitions. However, no broad emission band from the free ligand is observed, which indicates that the ligand transfers the absorbed energy effectively to the emitting level of the metal center. The symmetry forbidden transition of $^5D_0 \rightarrow {}^7F_0$ (580 nm) shows that the Eu^{3+} ions in polymer 4 have the noncentrosymmetric coordination environment.[24] As

is well known, the $^5D_0 \rightarrow {}^7F_1$ transition is magnetic dipole in nature and less sensitive to its environment, while $^5D_0 \rightarrow {}^7F_2$ is electric dipole in origin and its intensity is strongly influenced by the crystal field.[25,26] It is noted that the intensity of the $^5D_0 \rightarrow {}^7F_2$ transition is ca. 2.8 times of the intensity of the $^5D_0 \rightarrow {}^7F_1$ transition, which suggests that the Eu^{3+} ions occupy low symmetry coordination site with no inversion center, in consistent with the result from crystallographic analyses. In addition, the red emission of $^5D_0 \rightarrow {}^7F_2$ transition is the most intense, which indicates that the H_2mbpdc ligands are suitable for sensitization of red luminescence for Eu^{3+} ion under the experimental conditions, as observed in the literature.[24] When H_2mbpdc ligand is introduced to sensitize the Tb^{3+} ion, the emission spectrum of **6** exhibits the two characteristic emission bands of Tb^{3+} ion. They are assigned to the $^5D_4 \rightarrow {}^7F_J$ (J = 5, 6), $^5D_4 \rightarrow {}^7F_6$ (489 nm) and $^5D_4 \rightarrow {}^7F_5$ (535 nm) transitions. However, there is a very intense broad background in the excitation spectrum of 6, which means there exists intramolecular $\pi \rightarrow \pi^*$ transition of ligands. This luminescent phenomenon was observed in terbium complexes.[29]

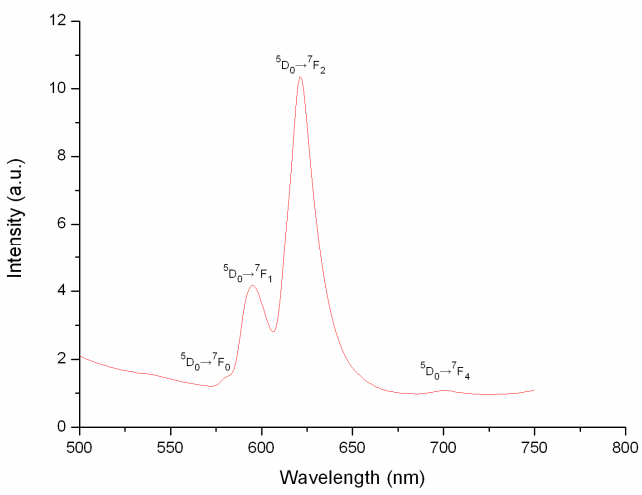

(a)

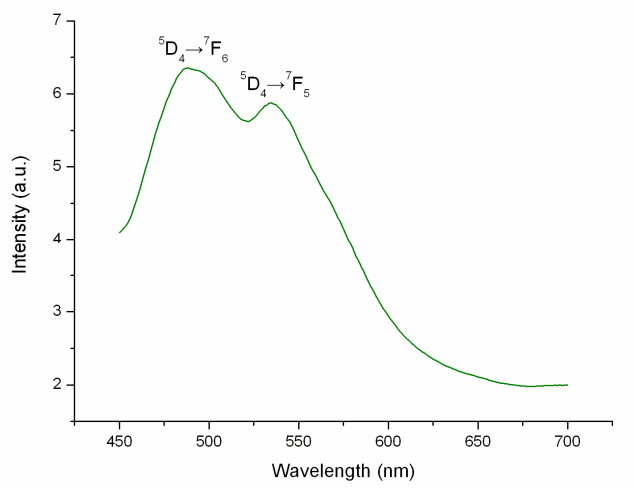

(b)

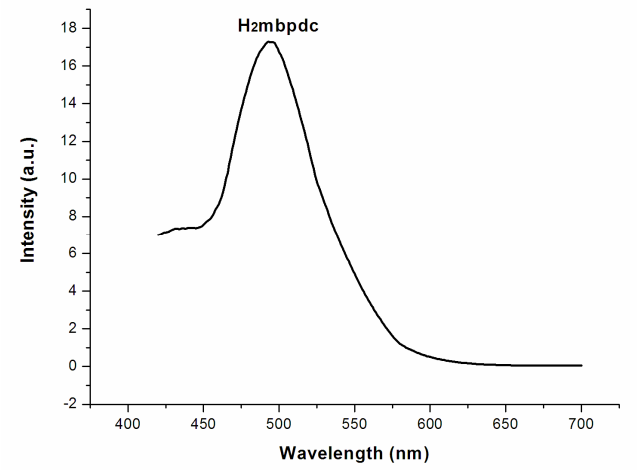

(c)

Figure 5. Solid-state emission spectra of **4** (a), **6** (b) and ligand (c) at room temperature.

Magnetic Properties.

The temperature-dependent magnetic susceptibilities of **6**–**8** were measured with an applied magnetic field of 1000 Oe at the temperatures range of 2-300 K. The $\chi_M T$ value of 11.43, 14.05 and 13.80 $cm^3 \cdot K \cdot mol^{-1}$ at room temperature for **6**–**8** (Figure 6), respectively, is slightly lower than the corresponding expected value of 11.82, 14.17 and 14.07 $cm^3 \cdot K \cdot mol^{-1}$ for one isolated Tb^{3+} (S = 3, L = 3, $^7F_6$, g = 3/2)[28], Dy^{3+} (S = 5/2, L = 5, $^6H_{15/2}$, g = 4/3)[29] and Ho^{3+} (S = 2, L = 6, $^5I_8$, g = 5/4)[30]. As the temperature cooling, the $\chi_M T$ values of **6** and **7** gradually declines to 9.18 and 11.38 $cm^3 \cdot K \cdot mol^{-1}$ at 2 K, respectively. The value of **8** slowly decreases to 10.38

$cm^3 \cdot K \cdot mol^{-1}$ at 25 K. and then sharply drops to 5.87 $cm^3 \cdot K \cdot mol^{-1}$ at 2 K with further cooling. Although compounds **6**, **7** and **8** are isomorphous, the different magnetic behavior at low temperature may originate from their different M_J sublevels.

As well known, the coupling between the lanthanide ions is relatively weak due to the efficient shielding of the unpaired electrons in their 4f orbitals. Significant coupling of lanthanide ions usually involves one or two atom bridges. For compounds **6–8**, the carboxylic bridges amongst metal ions poorly mediate the magnetic interactions. The metal ions are quite far apart from each other with the shortest Ln···Ln distances of 6.0694(4) Å, 6.0483(4) Å, and 6.0561(3) Å, respectively, indicating that magnetic coupling between the lanthanide ions is likely to be rather weak. On the other hand, the inter-electronic repulsion and the spin-orbit coupling lead to the 4fn electron configurations of the lanthanide ions splitting into $2S+1L_J$ states and further into M_J sublevels due to the crystal field perturbation. These sublevels are thermally populated at room temperature[31], and the progressive depopulations occur when the temperature decreases, causing the $\chi_M T$ value of lanthanide ions drop. As a result, the overall behaviors of $\chi_M T$ for **6–8** are mainly ascribed to thermal depopulation of the excited M_J sublevels split by the crystal field.

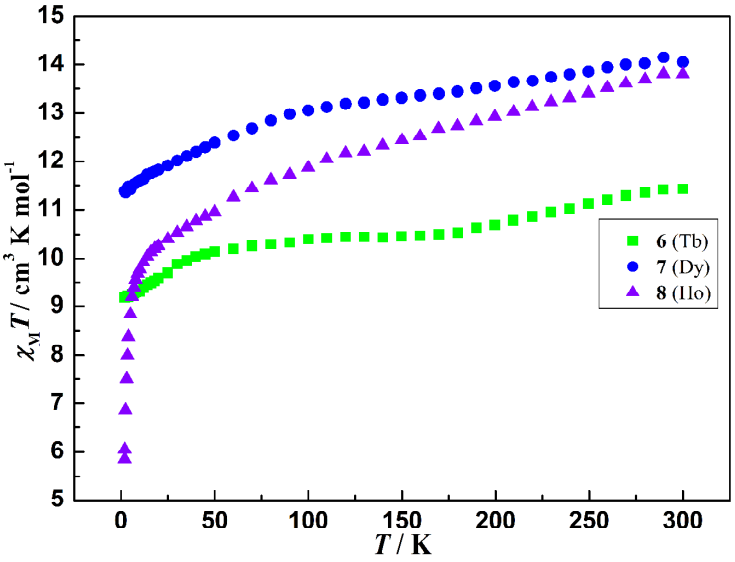

Figure 6. The plots of $\chi_M T$ *vs* T for compounds **6**, **7** and **8**.

Conclusions.

In summary, we have synthesized ten novel coordination polymers based on lanthanide ions and 3,3'-dimethoxy-2,2'-bipyridine-6,6'-dicarboxylic acid (H_2mbpdc) through an *in-situ* ligand transformation reaction. These polymers display three new structural types, from three to two-dimensional frameworks with respective nodes as the Ln^{3+} radii decrease. Polymers **1**–**3** exhibit highly ordered 3D frameworks with unprecedented 2D entangled layers of warp-and-woof threads interwoven by left- and right-handed helical chains (type I). While **4**–**10** show 2D 4^4 grids (type II and type III). Moreover, polymers **4** and **6** exhibit strong red and green photoluminescence at room temperature, respectively. The magnetic properties of compounds **6**–**8** were also studied by measuring their magnetic susceptibility over the temperature range of 2-300 K.

Experimental Section

Materials and Physical Techniques.

All chemicals were used as received without further purification. 3,3'-dimethoxy-2,2'-bipyridine-6,6'-dicarboxylic acid (H_2mbpdc) was prepared by the method described in the literature.[21] The hydrothermal syntheses of **1**–**10** were carried out in 23 mL Teflon-lined autoclaves under autogenous. Element analyses for C, H, and N were performed on a Flash 1112 elemental analyzer. The infrared spectra were recorded on a Nicolet Avatar-360 spectrophotometer with pressed KBr pellets. Powder X-ray diffraction (PXRD) patterns were recorded using a Rigaku D/Max-IIIA diffractometer from 5 to 50° with a step size of 0.01052° and a scan speed of 0.4s preset time. TGA (thermal gravimetric analyses) were carried out under nitrogen on a SDT Q600 with a heating rate of 2 °C/min. Luminescent spectra were recorded with a Hitachi F4500 fluorescence spectrophotometer. The variable-temperature magnetic susceptibility measurements were carried out on polycrystalline samples on a Quantum Design MPMS-7 SQUID magnetometer in the temperature range of 2–300 K. Diamagnetic corrections were made with Pascal's constants for all of the

constituent atoms.

Synthesis of the Coordination Polymers.

All ten polymers were prepared by the same synthetic routes, as follows: An aqueous mixture containing $Ln(NO_3)3•6H_2O$ (Ln = La, Ce, Pr, Eu, Gd, Tb, Dy, Ho, Er, and Lu, 0.2 mmol), and H_2mbpdc ligand (18.0 mg, 0.2 mmol) was allowed to place in a Parr Teflonlined stainess steel vessel (23 mL), and the vessel was sealed and heated to 180 °C for 3 days, then cooled to room temperature at a rate of 5 °C h^{-1}. The suitable crystals of **1**–**10** were collected directly. For **1**, yield: 0.036g, 42% based on La. Anal. Calcd (%) for $C_{12}H_7LaN_2O_7$: C, 33.51; H, 1.64; N, 6.51. Found: C, 33.69; H, 1.81; N, 6.67. For **2**, yield: 0.037g, 43% based on Ce. Anal. Calcd (%) for $C_{12}H_7CeN_2O_7$: C, 33.42; H, 1.64; N, 6.49. Found: C, 33.58; H, 1.74; N, 6.76. For **3**, yield: 0.048g, 55% based on Pr. Anal. Calcd (%) for $C_{12}H_7PrN_2O_7$: C, 33.46; H, 1.63; N, 6.48. Found: C, 33.56; H, 1.74; N, 6.68. For **4**, yield: 0.044g, 48% based on Eu. Anal. Calcd (%) for $C_{12}H_9EuN_2O_8$: C, 31.25; H, 1.97; N, 6.07. Found: C, 31.45; H, 2.12; N, 6.18. For **5**, yield: 0.056g, 60% based on Gd. Anal. Calcd (%) for $C_{12}H_9GdN_2O_8$: C, 30.90; H, 1.94; N, 6.01. Found: C, 31.25; H, 2.15; N, 6.19. For **6**, yield: 0.056g, 66% based on Tb. Anal. Calcd (%) for $C_{12}H_9TbN_2O_8$: C, 30.79; H, 1.94; N, 5.98. Found: C, 31.05; H, 2.17; N, 6.15. For **7**, yield: 0.064g, 68% based on Dy. Anal. Calcd (%) for $C_{12}H_9DyN_2O_8$: C, 30.55; H, 1.92; N, 5.94. Found: C, 30.85; H, 2.12; N, 6.17. For **8**, yield: 0.064g, 63% based on Ho. Anal. Calcd (%) for $C_{12}H_9HoN_2O_8$: C, 30.40; H, 1.91; N, 5.91. Found: C, 30.65; H, 2.09; N, 6.11. For **9**, yield: 0.066g, 69% based on Er. Anal. Calcd (%) for $C_{12}H_9ErN_2O_8$: C, 30.25; H, 1.90; N, 5.88. Found: C, 30.45; H, 2.04; N, 5.98. For **10**, yield: 0.062g, 64% based on Lu. Anal. Calcd (%) for $C_{12}H_9LuN_2O_8$: C, 29.77; H, 1.87; N, 5.79. Found: C, 30.45; H, 2.04; N, 5.98.

Crystallographic Analyses. Crystallographic data of **1**–**10** were collected on a Bruker Smart Apex-II CCD area detector at room temperature (graphite-monochromated, Mo Kα-radiation, ω- and θ-scan technique, λ = 0.71073 Å). An empirical absorption correction was applied. The structures were solved by direct

methods and refined on F^2 using SHELXTL package.[32,33] All non-hydrogen atoms were refined anisotropically. The hydrogen atoms were set in calculated positions and refined as riding atoms with a common isotropic thermal parameter. The crystallographic data for **1–10** are listed in Table 4. CCDC 975869 (**1**), 975870 (**2**), 975871 (**3**), 975872 (**4**), 975873 (**5**), 975874 (**6**), 975875 (**7**), 975876 (**8**), 975877 (**9**), and 975878 (**10**) contain the supplementary crystallographic data. These materials can be obtained free of charge via www.ccdc.cam.ac.uk/conts/retrieving.html (or from the Cambridge Crystallographic Data Center, 12 Union Road, Cambridge CB2 1EZ, UK; fax: (44) 1223 336-033. E-mail: deposit@ccdc.cam.ac.uk).

Acknowledgements.

We are grateful to the Natural Science Foundations of China (Grant No. 21372112 and 21272109) and the science and technology innovation team support programs of Henan Province University (No. 2012IRTSTHN019) for financial support.

Table 4. Crystallographic data and structure refinement summary for polymers **1–10**

	1	**2**	**3**	**4**	**5**
Formula	$C_{12}H_7LaN_2O_7$	$C_{12}H_7CeN_2O_7$	$C_{12}H_7PrN_2O_7$	$C_{12}H_9EuN_2O_8$	$C_{12}H_9GdN_2O_8$
M	430.11	431.32	432.11	461.17	466.46
Cryst syst	Monocline	Monocline	Monocline	Monocline	Monocline
Space group	*C*c	*C*c	*C*c	*C*c	*C*c
a(Å)	17.724(3)	17.604(16)	17.570(3)	17.909(3)	17.858(3)
b(Å)	10.6818(15)	10.624(9)	10.6061(15)	10.2645(15)	10.2355(15)
c(Å)	7.0003(10)	6.996(6)	6.9846(10)	7.4561(11)	7.4678(11)
α(°)	90	90	90	90	90
β(°)	111.839(10)	111.663(8)	111.5980(10)	96.9570(10)	96.909(2)
γ(°)	90	90	90	90	90
V(Å^3)	1230.2(3)	1216.1(19)	1210.2(3)	1360.5(3)	1355.1(3)
Z	4	4	4	4	4
D_{calc}(g cm^{-3})	2.322	2.356	2.372	2.251	2.286
μ(mm^{-1})	3.514	3.785	4.069	4.658	4.942
F(000)	824	828	832	888	892
data/params	4627 / 2254	4455 / 2229	4500 / 2208	4096 / 2296	4382 / 2425

GOF on F^2	1.022	1.080	1.086	1.024	1.128
$R_1(I > 2\sigma)$	0.0143	0.0149	0.0148	0.0171	0.0181
$wR_2(I > 2\sigma)$	0.0386	0.0397	0.0379	0.0419	0.0469
dimensionality	3D network			2D grid	

	6	**7**	**8**	**9**	**10**
Formula	$C_{12}H_9TbN_2O_8$	$C_{12}H_9DyN_2O_8$	$C_{12}H_9HoN_2O_8$	$C_{12}H_9ErN_2O_8$	$C_{12}H_9LuN_2O_8$
M	468.13	471.71	474.14	476.47	484.18
Cryst syst	Orthorhombic	Orthorhombic	Orthorhombic	Orthorhombic	Orthorhombic
Space group	*Pbcn*	*Pbcn*	*Pbcn*	*Pbcn*	*Pbcn*
a(Å)	8.4886(11)	8.439(2)	8.446(4)	8.4022(15)	8.3414(10)
b(Å)	20.972(3)	20.933(5)	21.009(10)	20.939(4)	20.948(3)
c(Å)	8.0409(10)	8.016(2)	8.016(4)	7.9883(14)	7.9372(10)
V(Å^3)	1431.4(3)	1416.0(6)	1422.4(12)	1405.4(4)	1386.9(3)
Z	4	4	4	4	4
D_{calc}(g cm^{-3})	2.172	2.213	2.214	2.252	2.319
μ(mm^{-1})	4.986	5.323	5.608	6.018	7.165
F(000)	896	900	904	908	920
data/params	9879 / 1335	9575 / 1314	8996 / 1323	9727 / 1304	5910 / 2925
GOF on F^2	1.036	1.061	1.086	1.046	1.079
$R_1(I > 2\sigma)$	0.0168	0.0179	0.0148	0.0147	0.0150
$wR_2(I > 2\sigma)$	0.0397	0.0395	0.0379	0.0319	0.0368
dimensionality	2D grid				

References

1 S. I. Weissman, *J. Chem. Phys.* **1942**, *10*, 214–217.

2 (a) D. Parker, *Coord. Chem. Rev.* **2000**, *205*, 109–130; (b) N. Sabbatini, M. Guardigli and J. M. Lehn, *Coord. Chem. Rev.* **1993**, *123*, 201–228; (c) J. Kido and Y. Okamoto, *Chem. Rev.* **2002**, *102*, 2357–2368.

3 (a) H. C. Aspinall, *Chem. Rev.* **2002**, *102*, 1807–1850; (b) M. Shibasaki and N. Yoshikawa, *Chem. Rev.* **2002**, *102*, 2187–2209; (c) R. J. Hill, D. L. Long, N. R. Champness, P. Hubberstey and M. Schroder, *Acc. Chem. Res.* **2005**, *38*, 335–348; (d) J. C. G. Bunzli and C. Piguet, *Chem. Soc. Rev.* **2005**, *34*, 1048–1077.

4 (a) L. Pan, K. M. Adams, H. E. Hernandez, X. Wang, C. Zheng, Y. Hattori and K. Kaneko, *J. Am. Chem. Soc.* **2003**, *125*, 3062–3067; (b) J. B. Yu, L. Zhou, H. J. Zhang, Y. X. Zheng, H. R. Li, R. P. Deng, Z. P. Peng and Z. F. Li, *Inorg. Chem.*

2005, *44*, 1611–1618; (c) J. Yang, Q. Yue, G. D. Li, J. J. Cao, G. H. Li and J. S. Chen, *Inorg. Chem*. **2006**, *45*, 2857–2865; (d) L. Z. Zhang, W. Gu, B. Li, X. Liu and D. Z. Liao, *Inorg. Chem*. **2007**, *46*, 622–624; (e) X. Q. Zhao, P. Cui, B. Zhao, W. Shi and P. Cheng, *Dalton Trans*., **2011**, *40*, 805–819; (f) P. F. Shi, B. Zhao, G. Xiong, Y. L. Hou and P. Cheng, *Chem. Commun*. **2012**, *48*, 8231–8233.

5 (a) Z. Zheng, *Chem. Commun*. **2001**, 2521–2529; (b) M. R. Bürgstein, M. T. Gamer and P. W. Roesky, *J. Am. Chem. Soc*. **2004**, *126*, 5213–5218; (c) R. C. Evans, P. Douglas and C. J. Winscom, *Coord. Chem. Rev*. **2006**, *250*, 2093–2126; (d) L. Candillas-Delgado, O. Fabelo, C. Ruiz-Perez, F. S. Delgado, M. Julve, M. Hernandez-Molina, M. Milagros Laz and P. Lorenzo-luis, *Cryst. Growth Des*. **2006**, *6*, 87–93; (e) E. Deiters, B. Song, A. S. Chauvin, C. D. B. Vandevyver, F. Gumy and J. C. G. Bunzli, *Chem. Eur. J*. **2009**, *15*, 885–900; (f) P. F. Shi, Y. Z. Zheng, X. Q. Zhao, G. Xiong, B. Zhao, F. F. Wan and P. Cheng, *Chem. Eur. J*. **2012**, *18*, 15086–15091; (g) P. F. Shi, G. Xiong, B. Zhao, Z. Y. Zhang and P. Cheng, *Chem. Commun*. **2013**, *49*, 2338–2340.

6 (a) J. Kido and Y. Okamoto, *Chem. Rev*. **2002**, *102*, 2357–2368; (b) N. Marques, A. Sella and J. Takats, *Chem. Rev.* **2002**, *102*, 2137–2160; (c) J. C. G. Bünzli and C. Piguet, *Chem. Soc. Rev*. **2005**, *34*, 1048–1077; (d) A. Y. Robin and K. M. Fromm, *Coord. Chem. Rev*. **2006**, *250*, 2127–2157; (e) H. Kobayashi, M. Ogawa, R. Alford, P. L. Choyke and Y. Urano, *Chem. Rev*. **2010**, *110*, 2620–2640; (f) M. D. Allendorf, C. A. Bauer, R. K. Bhakta and R. J. T. Houk, *Chem. Soc. Rev*. **2009**, *38*, 1330–1352; (g) J. C. G. Bunzli, *Chem. Rev*. **2010**, *110*, 2729–2755.

7 (a) B. Moulton and M. J. Zaworotko, *Chem. Rev*. **2001**, *101*, 1629–1658; (b) J. C. G. Bünzli and C. Piguet, *Chem. Rev*. **2002**, *102*, 1897–1928; (c) F. A. A. Paz and J. Klinowski, *Chem. Commun*. **2003**, 1484–1485; (d) X. Guo, G. Zhu, Q. Fang, M. Xue, G. Tian, J. Sun, X. Li and S. Qiu, *Inorg. Chem*. **2005**, *44*, 3850–3855; (d) J. Xia, B. Zhao, H. S. Wang, W. Shi, Y. Ma, H. B. Song, P. Cheng, D. Z. Liao and S. P. Yan, *Inorg. Chem*. **2007**, *46*, 3450–3458; (e) L. Huang, L. J. Han, W. J. Feng, L. Zheng, Z. B. Zhang, Y. Xu, Q. Chen, D. R Zhu and. S. Y. Niu, *Cryst. Growth Des*. **2010**, *10*, 2548–2552.

8 (a) L. Pan, X. Huang, J. Li, Y. Wu and N. Zheng, *Angew. Chem. Int. Ed*. **2000**, *39*, 527–530; (b) A. Dimos, D. Tsaousis, A. Michaelides, S. Skoulika, S. Golhen, L. Ouahab, C. Didierjean and A. Aubry, *Chem. Mater*. **2002**, *14*, 2616–2622; (c) Z. He, E. Gao, Z. Wang, C. Yan and M. Kurmoo, *Inorg. Chem*. **2005**, *44*, 862–874; (d) F. N. Shi, L. Cunha-Silva, R. A. Sá Ferreira, L. Mafra, T. Trindade, L. D. Carlos, F. A. Almeida Paz and J. Rocha, *J. Am. Chem. Soc*. **2008**, *130*, 150–167.

9 (a) W. Shi, X. Chen, Y. Zhao, B. Zhao, P. Cheng, A. Yu, H. Song, H. Wang, D. Liao, S. Yan and Z. Jiang, *Chem. Eur. J*. **2005**, *11*, 5031–5039; (b) J. W. Cheng, S. T. Zheng and G. Y. Yang, *Dalton Trans*. **2007**, 4059–4066.

10 (a) F. A. Cotton, G. Wilkinson, C. A. Murrillo and M. Bochmann, *Advanced Inorganic Chemistry*, 6th ed. Wiley, New York, **1999**, pp. 1108; (b) S. Mizukami, H. Houjou, M. Kanesato and K. Hiratani, *Chem. Eur. J*. **2003**, *9*, 1521–1528; c) B. Liu, W. P. Wu, L. Hou and Y. Y. Wang, *Chem. Commun*. **2014**, *50*, 8731–8734; d) L. N. Jia, L. Hou, L. Wei, X. J. Jing, B. Liu, Y. Y. Wang and Q. Z. Shi, *Cryst. Growth Des.* **2013**, *13*, 1570–1576.

11 C. M. Liu, M. Xiong, D. Q. Zhang, M. Du and D. B. Zhu, *Dalton Trans*. **2009**, 5666–5672.

12 (a) M. S. Liu, Q. Y. Yu, Y. P. Cai, C.Y. Su, X. M. Lin, X. X. Zhou and J. W. Cai, *Cryst. Growth Des*. **2008**, *8*, 4083–4091; (b) Y. W. Wang, Y. L. Zhang, W. Dou, A. J. Zhang, W. W. Qin and W. S. Liu, *Dalton Trans.* **2010**, *39*, 9013–9021; (c) W. G. Lu, L. Jiang and T. B. Lu, *Cryst. Growth Des*. **2010**, *10*, 4310–4318: (d) J. Lin, P. Chai, K. Diefenbach, M. Shatruk, T. E. Albrecht-Schmitt, *Chem. Mater*. **2014**, *26*, 2187_2194; (e) J. Lin, K. Diefenbach, N. Kikugawa, R. E. Baumbach, T. E. Albrecht-Schmitt, *Inorg. Chem*. **2014**, *53*, 8555–8564.

13 (a) A. Dimos, D. Tsaousis, A. Michaelides, S. Skoulika, S. Golhen, L. Ouahab, C. Didierjean and A. Aubry, *Chem. Mater*. **2002**, *14*, 2616–2622; (b) S. Mizukami, H. Houjou, M. Kanesato and K. Hiratani, *Chem Eur. J*. **2003**, *9*, 1521–1528; (c) Z. He, E. Gao, Z. Wang, C. Yan and M. Kurmoo, *Inorg. Chem*. **2005**, *44*, 862–874; (d) J. W. Cheng, T. S. Zheng and G. Y. Yang, *Dalton Trans*. **2007**, *36*, 4059–4066; (e) Y. H. Wan, X. J. Zheng, F. Q. Wang, X. Y. Zhou, K. Z. Wang and

L. P. Jin, *CrystEngComm*, **2009**, *11*, 278–283.

14 (a) A. Huignard, T. Gacoin and J. P. Boilot, *Chem. Mater*. **2000**, *12*, 1090–1094; (b) W. L. Fan, Y. X. Bu, X. Y. Song, S. X. Sun and X. Zhao, *Cryst. Growth Des*. **2007**, *7*, 2361–2366; (c) C. Marchal, Y. Filinchuk, X. Y. Chen, D. Imbert and M. Mazzanti, *Chem Eur. J*. **2009**, *15*, 5273–5288; (d) L. W. Qian, J. Zhu, Z. Chen, Y. C. Gui, Q. Gong, Y. P. Yuan, J. T. Zai and X. F. Qiang, *Chem Eur. J*. **2009**, *15*, 1233–1240; (e) Z. J. Zhang, S. Y. Zhang, Y. Li, Z. Niu, W. Shi and P. Cheng, *CrystEngComm*, **2010**, *12*, 1809–1815.

15 (a) J. Jia, X. Lin, A. J. Blake, N. R. Champness, P. Hubberstey, L. Shao, G. Walker, C. Wilson and M. Schröder, *Inorg. Chem*. **2006**, *45*, 8838–8840; (b) B. L. Chen, L. B. Wang, Y. Q. Xiao, F. R. Fronczek, M. Xue, Y. J. Cui and G. D. Qian, *Angew. Chem. Int. Ed*. **2009**, *48*, 500–503; (c) S. L. Xiang, J. Huang, L. Li, J. Y. Zhang, L. Jiang, X. J. Kuang and C. Y. Su, *Inorg. Chem*. **2011**, *50*, 1743–1748.

16 (a) F. Q. Wang, X. J. Zheng, Y. H. Wan, C. Y. Sun, Z. M. Wang, K. Z. Wang and L. P. Jin, *Inorg. Chem*. **2007**, *46*, 2956–2958; (b) D. F. Weng, X. J. Zheng, X. B. Chen, L. Li and L. P. Jin, *Eur. J. Inorg. Chem*. **2007**, 3410–3415; (c) P. C. R. Soares-Santos, L. Cunha-Silva, F. A. Almeida Paz, R. A. S. Ferreira, J. Rocha, L. D. Carlos and H. I. S. Nogueira, *Inorg. Chem*., **2010**, *49*, 3428–3440.

17 (a) X. Li, B. L. Wu, C. Y. Niu, Y. Y. Niu and H. Y. Zhang, *Cryst. Growth Des*., **2009**, *9*, 3423–3421; (b) W. Y. Wang, Z. L. Yang, C. J. Wang, H. J. Lu, S. Q. Zang and G. Li, *CrystEngComm*., **2011**, *13*, 4895–4902; (c) S. L. Cai, S. R. Zheng, Z. Z. Wen, J. Fan and W. G. Zhang, *Cryst. Growth Des*. **2012**, *12*, 2355–2361.

18 (a) N. R. Kelly, S. Goetz, S. R. Batten and P. E. Kruger, *CrystEngComm.* **2008**, *10*, 68–78; (b) N. R. Kelly, S. Goetz, S. R. Batten and P. E. Kruger, *CrystEngComm.* **2008**, *10*, 1018–1026; (c) B. M. Ji, D. S. Deng, X. He, B. Liu, S. B. Miao, N. Ma, W. Z. Wang, L. G. Ji, P. Liu and X. F. Li, *Inorg. Chem*. **2012,** *51*, 2170–2177.

19 (a) J. R. Lombardi and B. Davis, *Chem. Rev.* **2002**, *102*, 2431–2460; (b) J. L. C. Rowsell and O. M. Yaghi, *Microporous Mesoporous Mater*. **2004**, *73*, 3–14.

20 (a) T. J. J. Kinnunen, M. Haukka and T. A. Pakkanen, *J. Organomet. Chem*. **2002**,

654, 8–15; (b) U. Dawid, F. P. Pruchnik and R. Starosta, *Dalton Trans*. **2009**, 3348–3353.

21 B. M. Ji, D. S. Deng, H. H. Lan, C. X. Du, S. L. Pan and B. Liu, *Cryst. Growth Des*. **2010**, *10*, 2851–2853.

22 (a) D. S. Deng, L. L. Liu, B. M. Ji, G. J. Yin and C. X. Du, Cryst. Growth. Des. 2012, 12, 5338–5342; (b) H. B. Zhu and S. H. Gou, *Coord. Chem. Rev*. **2011**, *255*, 318–338; (c) H. Zhao, Z. R. Qu, H. Y. Ye and R. G. Xiong, *Chem. Soc. Rev*. **2008**, *37*, 84–100; (d) X. D. Chen, H. F. Wu and M. Du, *Chem. Commun*. **2008**, 1296–1298; (e) X. M. Chen and M. L. Tong, *Acc. Chem. Res*. **2007**, *40*, 162–170.

23 (a) Y. H. Feng, Y. Guo, Y. O. Yang, Z. Q. Liu, D. Z. Liao, P. Cheng, S. P. Yan and Z. H. Jiang, *Chem. Commun*. **2007**, *43*, 3643–3645; (b) X. F. Wang, Y. B. Zhang, X. N. Cheng and X. M. Chen, *CrystEngComm.* **2008**, *10*, 753–758.

24 (a) B. Zhao, X. Y. Chen, P. Cheng, D. Z. Liao, S. P. Yan and Z. H. Jiang, *J. Am. Chem. Soc.* **2004**, *126*, 15394–15395; (b) X. J. Gu and D. F. Xue, *CrystEngComm.* **2007**, *9*, 471–477.

25 G. Vicentini, L. B. Zinner, J. Zukerman-Schpector and K. Zinner, *Coord. Chem. Rev*. **2000**, *196*, 353–382.

26 (a) A. F. Kirby, D. Foster and F. S. Richardson, *Chem. Phys. Lett*. **1983**, *95*, 507–512; (b) J. C. G. Bünzli and G. R. Choppin, in *Lanthanide Probes in life, Chemical and Earth Science. Theory and Practice*, Elsevier Scientific Publishers, Amsterdam, The Netherlands, 1989, ch. 7 (ref:1.2 IC).

27 (a) S. Raphael, M. L. P. Reddy, A. H. Cowley and M. Findlater, *Eur. J. Inorg. Chem*. **2008**, 4387–4394; (b) X. Yang, R. A. Jones and W. K. Wong, *Chem. Commun*. **2008**, 3266–3268.

28 C. A. Black, J. S. Costa, W. T. Fu, C. Massera, O. Roubeau, S. J. Teat, G. Aromi, P. Gamez and J. Reedijk, *Inorg. Chem.* **2009**, *48*, 1062–1068.

29 (a) Q. Y. Liu, W. F. Wang, Y. L. Wang, Z. M. Shan, M. S. Wang and J. K. Tang, *Inorg. Chem.* **2012**, *51*, 2381–2392; (b) G. F. Xu, Q. L. Wang, P. Gamez, Y. Ma, R. Clerac, J. K. Tang, S. P. Yan, P. Cheng and D. Z. Liao, *Chem. Commun.* **2010**, *46*, 1506–1508; (c) Y. Liu, Z. Chen, J. Ren, X. Q. Zhao, P. Cheng and B. Zhao,

Inorg. Chem. **2012**, *51*, 7433–7435.

30 Z. Majeed, K. C. Mondal, G. E. Kostakis, Y. Lan, C. E. Anson and A. K. Powell, *Chem. Commun.* **2010**, *46*, 2551–2553.

31 M. Fang, B. Zhao, Y. Zuo, J. Chen, W. Shi, J. Liang and P. Cheng, *Dalton Trans.* **2009**, 7765–7770.

32 *SHELXTL*, Version 5.1; Bruker AXS: Madison, WI, **1998**.

33 G. M. Sheldrick, *SHELXS-97 and SHELXL-97, Program for X-ray Crystal Structure Solution,* University of Göettingen, Germany, 1997.

Two- and Three-Dimensional Lanthanide-Based Coordination Polymers Assembled by the Synergistic Effect of Various Lanthanide Radii and Flexibility of a New Binicotinate-Containing Ligand: in Situ Synthesis, Structures, and Properties

Baoming Ji,[a*] Dongsheng Deng,[a] Junying Ma,[b] Chaowei Sun,[a,b] Bin Zhao[c*]

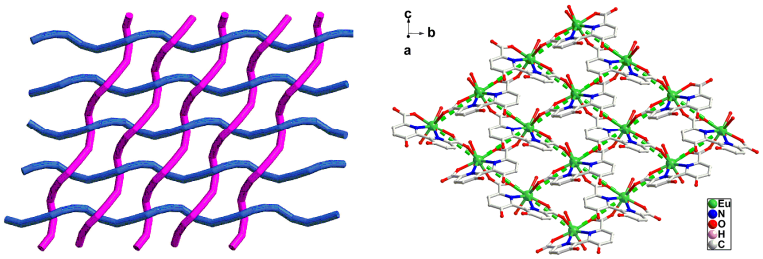

The design and synthesis of ten novel coordination polymers was investigated. The study indicates that they have three structural types from 3D to 2D polymers due to the synergistic effect of lanthanide contraction with diverse coordination modes and conformations of the ligand.

* To whom correspondence should be addressed. E-mail: lyhxxjbm@126.com